Construction and Building Materials 114 (2016) 763–771

Contents lists available at ScienceDirect

Construction and Building Materials

journal homepage: www.elsevier.com/locate/conbuildmat

Creep behaviors and constitutive model for high density polyethylene geogrid and its application to reinforced soil retaining wall on soft soil foundation

Chao Zou, Yimin Wang, Junyong Lin, Yekai Chen *

School of Civil Engineering and Transportation, South China University of Technology, Guangzhou, Guangdong 510541, China

HIGHLIGHTS

- Creep behavior and stress relaxation of geogrids have been investigated.
- Constitutive model for simulating creep behaviors and stress relaxation of geogrids.
- Working stress of geogrids should be less than 40% of ultimate tensile strength.
- Piles treated deep soft soil foundation can ignore creep behavior of soft soil.

ARTICLE INFO

Article history:
Received 15 May 2015
Received in revised form 28 March 2016
Accepted 29 March 2016

Keywords:
Geogrid
Creep
Soft soil
Reinforced retaining wall
Constitutive model

ABSTRACT

The reinforced soil retaining wall has been applied extensively with its numerous advantages. However, the performance of geogrids reinforced soil retaining wall was affected by creep behavior of geogrids and soft soil foundation as well as stress relaxation of geogrids. In this paper, the creep behavior and stress relaxation of high density polyethylene geogrids have been investigated in a laboratory. Four different sustained load levels of 20%, 40%, 50% and 60% of ultimate tensile strength were employed as load levels for creep tests. A constitutive model, which was capable of simulating creep behaviors and stress relaxation of geogrids, was established based on experimental data and verified. Numerical modeling using finite element method has also been used to assess the impact of creep behavior and stress relaxation of geogrids on the long-term performance of reinforced soil retaining wall on the deep soft soil foundation. The results show that the constitutive model for creep behavior and stress relaxation of geogrids was in good qualitative agreement with experimental data under different load levels. To ensure the stability of the retaining wall, the working stress of geogrids should be less than 40% of ultimate tensile strength, and the high strength geogrids should be adopted in the middle of the wall or the spacing of geogrid reinforced layers should be reduced. The deep soft soil foundation which is treated by piles can ignore the creep behavior of soft soil.

1. Introduction

Plastics geogrids, a type of geosynthetic, refer to high strength and durability polymer materials developed for reinforced retaining wall on the soft soil foundation [1]. For reinforced soil, geogrids provide tension strength to bound soil and restrain excessive lateral displacement of soil. However, geogrids are subjected to time-dependent creep behavior and stress relaxation in a stretched state in actual projects, leading to variational internal stress and affect the long-term performance in reinforced structures such as loss of overall stability and excessive deformation [2]. Therefore, the long-term creep strain of geogrids must not exceed the allowable value and the reinforced structures should be restricted to a limited deformation to keep long-term stability [3]. In addition, the creep deformation of soft soil induced by secondary consolidation has influence on the creep behavior and stress relaxation of geogrids through friction and adhesion [32]. All of these key factors influence the long-term performance of reinforced soil retaining wall.

Numerous studies have been conducted on the performance of reinforced retaining walls on the solid foundation [4–9]. The different wall and backfill materials, the reinforced intensity and length, and geometry of reinforced soil structures were reported based on

* Corresponding author.
E-mail address: cheops@scut.edu.cn (Y. Chen).

http://dx.doi.org/10.1016/j.conbuildmat.2016.03.194
0950-0618/

reinforced mechanism and design methods of reinforced retaining wall. The soil pressure, displacement and stress distribution at base of reinforced retaining walls have been previously summarized. Based on the results of these studies, the design methods of present specifications for reinforced retaining walls were formed gradually [10,11].

This is not the case with reinforced retaining walls on the soft soil foundation, where the settlement or differential settlement are taken place in most reinforced soils [12–15]. However, reinforced retaining walls sustained almost no damage and the strain of reinforcement materials did not exceed the design standards. Therefore, current design methods for reinforced retaining walls on the solid foundation were not suitable for soft soil foundation.

For the creep model of geogrids, linear [17,18], hyperbolic [19] and polynomial [20] constitutive relations, which did not consider time-dependent behavior [16], were used commonly in most early numerical analysis of geogrids reinforced retaining wall. Currently, creep models used in finite element analysis including component models, rheological models and empirical models, and empirical models based on test data were widely adopted. Finnigan and Findley [18,21] developed an empirical equation based on experiments that both short-term and long-term creep behaviors of geosynthetics have been considered. Das [22] proposed an empirical equation of strain rate for geogrids which was modified from the empirical rheological models of soil developed by Singh and Mitchell [29]. Additionally, rheological models which combined of creep and stress relaxation have been widely used to study the stress relaxation of geosynthetics. Sawicki [23,24] developed a three parameters' creep model based on linear solid model comprised of a spring and Kelvin's model, and proposed a four parameters' rheological model by adding a plastic slider.

In this study, creep tests of geogrids have been conducted and the creep behavior and stress relaxation of geogrids subjected to different loadings were investigated. In addition, a constitutive model, which was capable of simulating creep behaviors and stress relaxation of geogrids, was established based on experimental data and verified by comparing experimental and calculated results. The model was then incorporated into a finite element model to simulate the long-term performance of a reinforced retaining wall on the deep soft soil foundation. The results provide useful information for analysis and evaluation of the long-term performance of geogrids reinforced structure on the deep soft soil foundation.

2. Materials and apparatus

2.1. Properties of geogrid

Tensile properties of high density polyethylene geogrid were evaluated according to the test procedure described in ASTM D 6637 [25]. Ten longitudinal and transverse ribs cut from geogrids were tested at a constant displacement rate of 20 mm/min, respectively, and the typical load-deformation curves are shown in Fig. 1. The average ultimate tensile strength is 39.91 kN/m for longitudinal ribs and 36.79 kN/m for transverse ribs, and the average elongation rate under the ultimate tensile strength is 9.53% on longitudinal direction and 11.27% on transverse direction. Therefore, loads were applied on longitudinal ribs of geogrids in creep tests, and the properties of specimens in longitudinal direction are listed in Table 1.

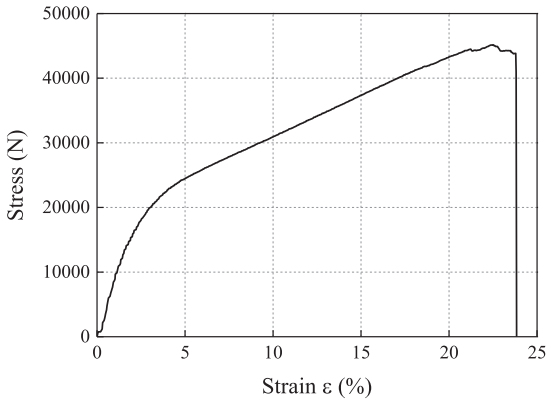

Fig. 1. Typical tensile behavior of geogrids.

Table 1
Longitudinal properties of specimens.

Properties	Specimen
Tensile strength (kN/m)	39.91
Strength at 2% strain (kN/m)	13.45
Strength at 5% strain (kN/m)	28.96
Width	3 ribs
Unit weight (kg/m^2)	0.6

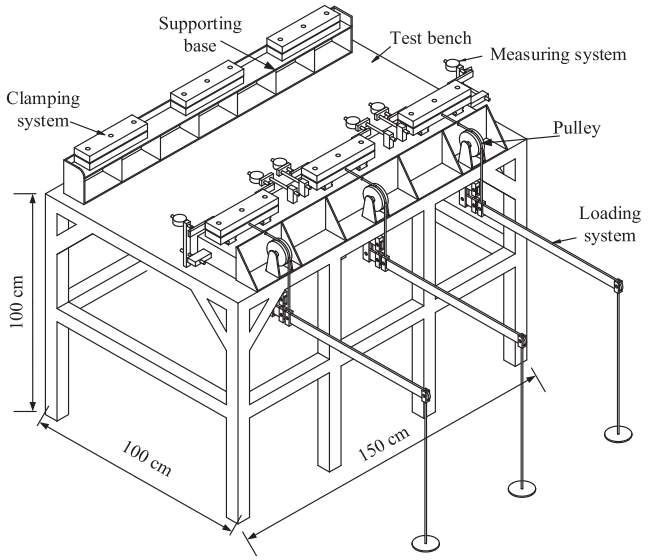

Fig. 2. Apparatus sketch for creep tests.

2.2. Description of apparatus

The test apparatus used in creep tests was developed by authors, which consisted of test bench, clamping system, loading system and measuring system, as shown in Fig. 2.

2.2.1. Test bench

The dimension of test bench is 1.5 × 1.0 × 1.0 m. Two stationary supporting bases were installed on each side of the test bench respectively, and one of them connected with pulley, which was used to convert vertical load to horizontal load.

2.2.2. Clamping system

Clamping system consisted of fixed fixtures and free fixtures, as shown in Fig. 3. All the fixtures were 30-cm-wide to ensure wider than specimens. It was easy to clamp the geogrid which has a thickness of 5 mm. However, clamping method was important to ensure the accuracy of test data. A non-slip treatment was used inside fixtures, and a row of bolts was set to provide clamping power. Fixtures connected with pulley were free to slide on the supporting base, and the other fixtures on another side of test bench were fixed. The specimen with three longitudinal parallel ribs was mounted inside the fixtures.

2.2.3. Loading system

Considering the difficulty of massive load application in the test, the principle of leverage with a scaling-down ratio of 1:8 was used to reduce the applied load. The load was applied to the specimens using weights, which were hung on the lever system as tensile load.

2.2.4. Measuring system

Two dial gauges were used for measuring the displacement of free fixtures to obtain deformation of specimen. Dial gauges, which have an accuracy of 0.01 mm, were mounted on both sides of the fixtures, as shown in Fig. 4.

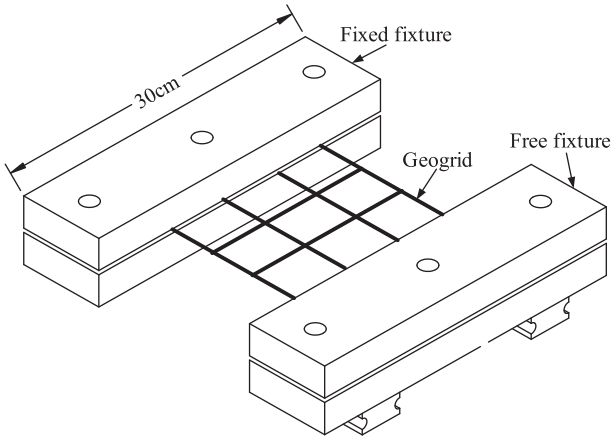

Fig. 3. Clamping system.

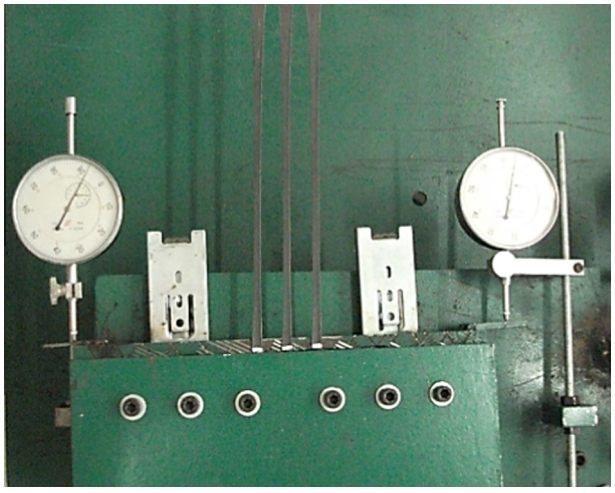

Fig. 4. Measuring system.

3. Experimental programme

3.1. Testing parameters

Creep strain ε is the ratio of elongation and initial length of the specimen under long-term static loading.

$$\varepsilon = \Delta L / L_0 \quad (1)$$

where ΔL is the change in length of specimen from the pretension force to the corresponding applied load at certain moment, mm; L_0 is the initial length plus the pretension displacement of specimen, mm.

Creep stress is the ratio of constant force and cross-sectional area perpendicular to the direction of constant force.

$$\sigma = F / S \quad (2)$$

where σ is creep stress; S is cross-sectional area of specimen; F is constant force that applied on the specimen in creep tests.

3.2. Testing environment

Creep tests were carried out in a laboratory in which temperature and humidity could be adjusted as needed. Keep the indoor temperature at 20 °C ± 2 °C and relative humidity between 50% and 70%.

Table 2
Load design for creep tests.

Ultimate load (KN/m)	Load level	Load (kN)	Weights (kg)
39.91	20%	0.92	93.97
	40%	1.84	187.95
	50%	2.30	234.94
	60%	2.76	281.92

3.3. Testing load

Four different sustained load levels employed for the creep tests were 20%, 40%, 50% and 60% of ultimate tensile strength, respectively, as listed in Table 2.

3.4. Data recording

The total time for creep tests was more than 720 h. In the first 24 h, the data were recorded at 0 min, 1 min, 2 min, 4 min, 8 min, 12 min, 30 min, 1 h, 2 h, 3 h, 4 h, 5 h, 10 h and 24 h, respectively. From then on, the data were recorded once every 24 h. To measure creep strain accurately, it was necessary to wait 1 min to record data after load application to eliminate the influence of elastic deformation of specimens on creep test results.

3.5. Testing program

The tests were carried out using the following steps:

(1) All specimens were equilibrated at temperature of 20 ± 2° and humidity of 60 ± 10% for 24 h.
(2) Mounted specimen inside the fixtures of clamping system, and a pre-stress was applied quickly and smoothly to the specimen. Recorded the elongation caused by pre-stress and used the value as the initial readings.
(3) Applied the weights as load rapidly and smoothly to each specimen, recorded dial gauge readings according to the schedule of data recording.

4. Test results and discussion

4.1. Creep curves under different load levels

Fig. 5 plots a series creep curves of geogrids. In all curves, the strain increased with the increased load levels and the deformational characteristic can be defined by power function. By applying 20% of ultimate tensile strength, the creep curve was relatively flat, and the strain was 1.655% at 720 h. By increasing load levels to

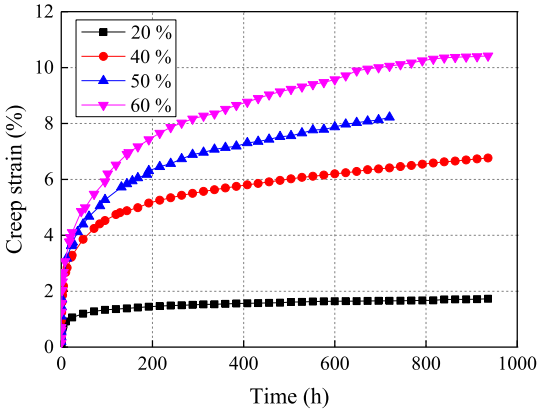

Fig. 5. Strain-time creep curves of geogrids.

40%, 50% and 60% of ultimate tensile strength respectively, the strain grew to 6.408%, 8.221% and 10.053% at 720 h, relatively. The increment of the creep strain between load levels of 40% and 20% was relatively greater than the one between load levels of 50% and 40%. It indicates that load level is an important factor affecting the creep behavior of geogrids, and 40% of ultimate tensile strength is a critical load. The working stress of geogrids should be less than 40% of ultimate tensile strength.

In addition, strain grew rapidly at the beginning, and finally became stabilized. The creep strain of geogrids became stabilized in a relatively shorter time with relatively smaller load levels, while those at the larger load levels were reversed. The reason is that the internal structure and molecular movement are easily changed with the high load levels application on geogrids.

4.2. Isochronous creep curves

Fig. 6 shows the isochronous load-strain curves of geogrids with similar trend under different load levels at 1 min, 1 h, 5 h, 24 h, 120 h, 240 h, 480 h, 600 h, and 720 h, respectively. At 1 min, the creep strains under different load levels were substantially equal, and the maximum value of the creep strain was 0.19%. At 720 h, the creep strain increased from 1.65% under load level of 20% to 10.05% under load level of 60%. It indicates that load is an important factor affecting the long-term creep behavior of geogrids, and heavy load may play a role in accelerating creep behavior.

4.3. Stress relaxation curves

Stress relaxation means that the strain remains constant while the stress gradually decreases with time [32]. Due to the indoor test of stress relaxation is difficult to control, the strain of 2.0%, 4.0% and 5.0% are selected to plot the curves of stress relaxation based on creep curves under different load levels, as shown in Fig. 7. The same trend at different strains and obvious stress relaxation were observed. The stress decreased rapidly at the beginning and then became stabilized gradually.

5. Constitutive model formulation of creep behavior and stress relaxation

5.1. Theory of constitutive model

The plastic behavior was observed obviously when high-stress ratios were applied to geogrids. Currently, most of creep models were hard to simulate the creep and stress relaxation of geogrids accurately and ignored to consider different load levels [3]. This

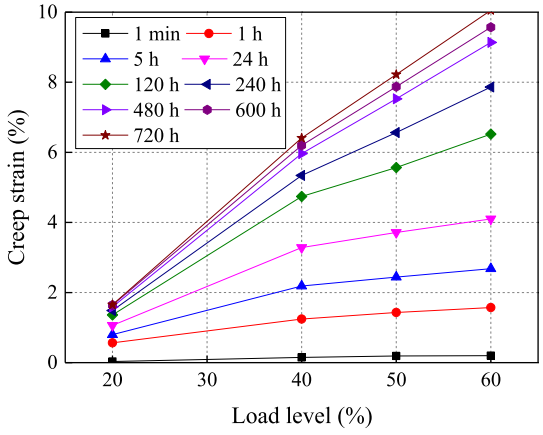

Fig. 6. Isochronous load-strain curves of geogrids.

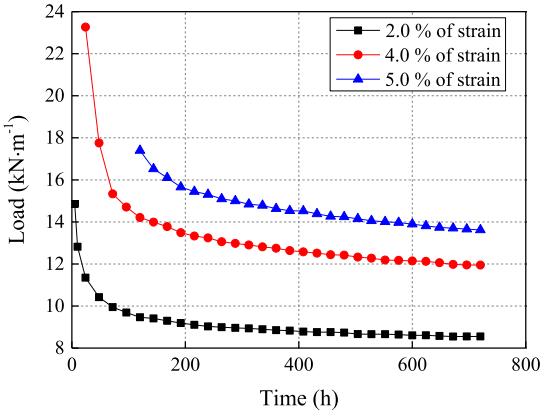

Fig. 7. Stress relaxation curves of geogrids.

paper uses creep model of metal as a reference and develops a time-dependent plastic deformation creep model for geogrids based on the creep tests [26].

Creep behavior is defined by the uniaxial creep, which is called creep law. For cohesive creep, creep law can be defined by time hardening formulation of power law:

$$\frac{\dot{\varepsilon}^{cr}}{\varepsilon} = A\sigma^n t^m \tag{3}$$

where $\frac{\dot{\varepsilon}^{cr}}{\varepsilon}$ is strain rate for equivalent creep; σ is stress for equivalent creep; t is total time; A, m, n are material constants. For physically reasonable behavior, A and n must be positive and $-1 \leqslant m \leqslant 0$.

Use the creep strain ε to replace the strain rate for equivalent creep, Eq. (3) will be changed into:

$$\varepsilon = \frac{A}{m+1}\sigma^n t^{m+1} \tag{4}$$

The constitutive modeling of creep behavior is given from Eq. (4):

$$\sigma = \varepsilon^{\frac{1}{n}}\left(\frac{m+1}{At^{m+1}}\right)^{\frac{1}{n}} \tag{5}$$

5.2. Parameters of constitutive modeling

Three parameters of A, m, n should be determined by creep tests. Convert Eq. (5) into natural logarithm form:

$$\ln\varepsilon = n\ln\sigma + \ln A + (m+1)\ln t - \ln(m+1) \tag{6}$$

The relationship of creep strain and stress and time can be changed into linearity in double logarithmic coordinates at a given moment. Thus, Eq. (6) can be written:

$$\ln\varepsilon = a\ln\sigma + b \tag{7}$$

$$\ln\varepsilon = c\ln t + d \tag{8}$$

where $a = n, b = (m+1)\ln t + nA - \ln(m+1), c = m+1, d = n\ln\sigma + \ln A - \ln(m+1)$.

Based on creep tests, the strain of geogrids under different load levels at representative moments are selected and the isochronal stress-strain relationships are plotted and linear fitted, as shown in Fig. 8 and Table 3. The fitted lines are essentially parallel to each other in logarithmic coordinate. It indicates that the slope a of fitted lines are approximately constant and time-independent, while the intercept of strain axis b of fitted lines are different and time-dependent. Thus, the average value of slope a is 0.68837, and n is 0.68837.

Table 3
Fitting parameter of stress-strain curves of geogrids at different moments.

Moment	Fitting equation	Correlation coefficient
1 min	y = 0.691x − 12.668	0.967
1 h	y = 0.6824x − 11.577	0.972
5 h	y = 0.685x − 11.022	0.971
24 h	y = 0.682x − 10.556	0.907
120 h	y = 0.698x − 10.073	0.989
240 h	y = 0.683x − 10.073	0.985
480 h	y = 0.693x − 10.107	0.976
600 h	y = 0.694x − 10.118	0.988
720 h	y = 0.683x − 9.966	0.989

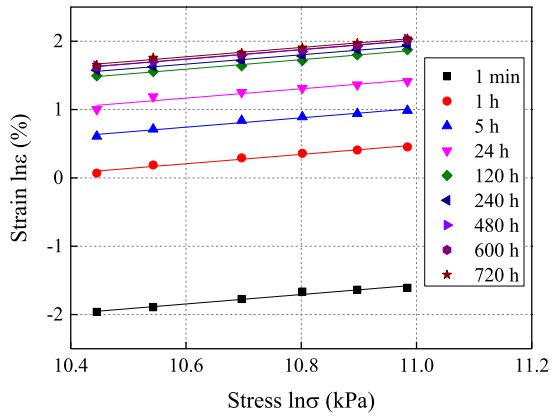

Fig. 8. Stress-strain curves of geogrids at different moments in logarithmic coordinate.

A series of strain-time curves of geogrids at different load levels in logarithmic coordinate are obtained and shown in Fig. 9. Each fitted line at different load levels is basically parallel to each other. Thus, the average value of slope c is 0.24283, and m is −0.75716.

According to Eq. (7), the intercept b is time-dependent and has a liner relationship with time t in logarithm. Therefore, the relationship between intercept b and time t is fitted and shown in Fig. 10. In this figure, $\ln A - \ln(m+1) = -11.54209$ and $A = 2.35857 \times 10^{-6}$.

Hence, the creep constitutive model formulation of geogrid is given as follows:

$$\sigma = \left(\frac{1.3573 \times 10^5 \varepsilon}{t^{0.2957}}\right)^{1.4286} \tag{9}$$

5.3. Validation and discussion of constitutive modeling

To validate the reasonableness and accuracy of the constitutive model, comparative analysis between the data of creep tests and simulation is shown in Fig. 11. It can be seen that the data obtained from tests and model simulation were basically equal. The creep model has the capacity to simulate the creep behavior of geogrids subject to high stress level. With the increase of load level, there was a small difference between the data of test and simulation, however, the maximum difference value of strain was only 0.239%. The proposed constitutive modeling can predict the creep strain of geogrids.

Fig. 12 shows the comparison of the stress relaxation between experimental and calculated results. It reveals that the proposed model is able to simulate the stress relaxation behavior of geogrids.

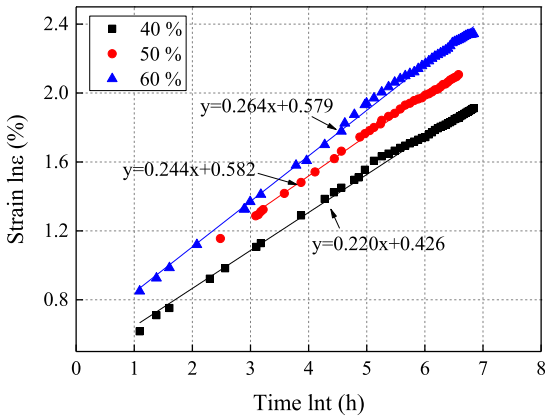

Fig. 9. Strain-time curves of geogrids in logarithmic coordinate.

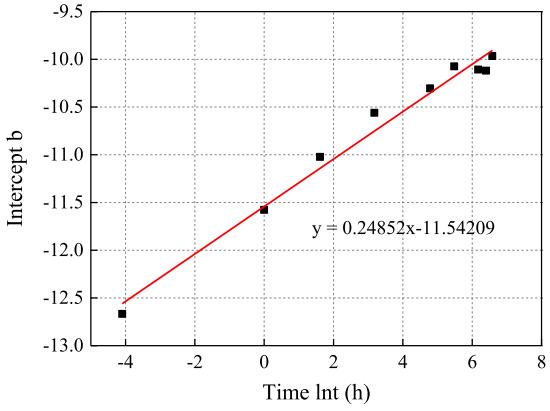

Fig. 10. Intercept-time relationship of geogrids.

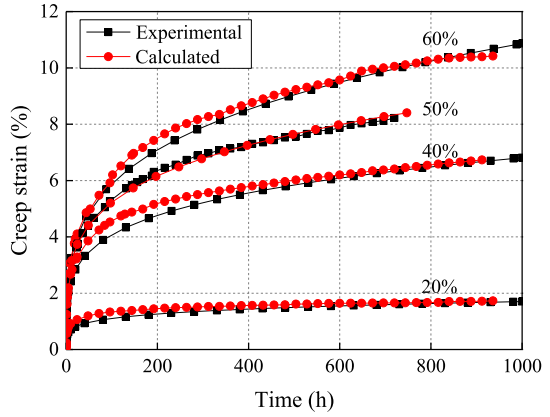

Fig. 11. Comparison between experimental and calculated creep strain.

6. Application of geogrids reinforced retaining wall

The proposed creep model of geogrids was applied to analyze the long-term behavior of geogrids reinforced retaining wall via the commercial finite element package ABAQUS [26]. An 8-m-high geogrids reinforced retaining wall was built on the deep soft soil foundation. The FE model is showed in Fig. 13.

The wall has a vertical hollow-block facing and assumed to be linear elastic with elasticity modulus of 9.8 GPa and density of 2700 kg/m^3 [27]. The reinforcement was 14 layers of geogrids with

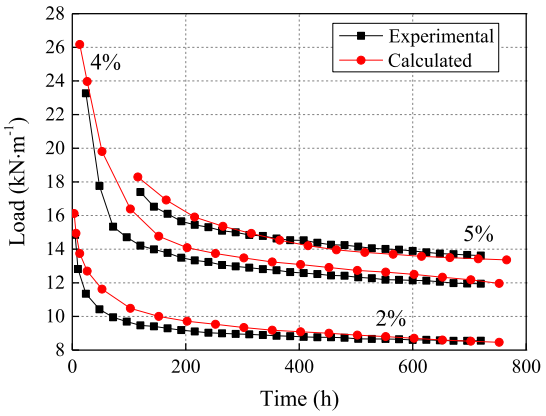

Fig. 12. Comparison between experimental and calculated data of stress relaxation.

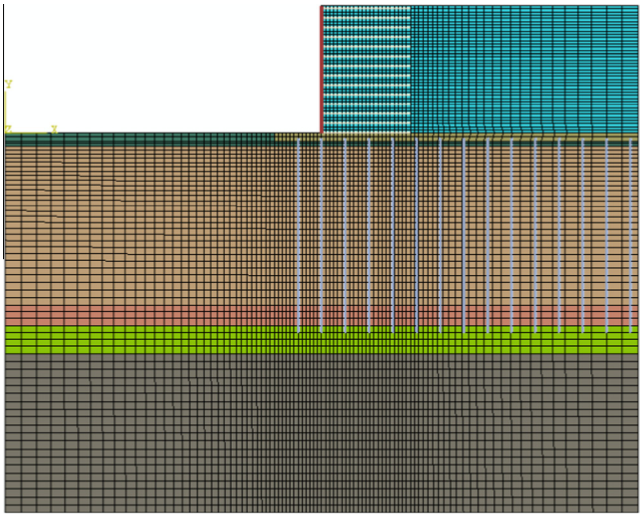

Fig. 13. Finite element model.

length of 5.6 m and spacing of 0.6 m. To limit relative movement of geogrids and wall, motion constraints were set at their contact points. The geogrids were modeled using aforementioned constitutive model and the parameters were showed in Table 1.

The distribution and parameters of backfill and foundation soils were listed in Table 4. The backfill soil and soft soil layer were modeled using modified Drucker-Prager creep model, and the parameters were obtained by retrieving field undisturbed soil samples to conduct triaxial compression tests and triaxial consolidated creep tests. Other soil layers were assumed to be linear elastic [28]. The interface of wall and backfill soil followed Mohr-Coulomb failure criterion. The horizontal displacement was constrained at the right side of the backfill soil and at the left and right side of the foundation soil, and horizontal and vertical displacement were constrained at the bottom of foundation soil.

Cement-flyash-gravel piles, which pile-spacing was 1.5 m and pile-diameter was 500 mm and pile-length was 12.1 m, were used to reinforce a 10-m-deep soft soil and assumed to be linear elastic.

In order to explore the impact of geogrids creep on long-term performance of retaining wall, the lateral displacement of wall, the surface settlement of foundation soil and backfill soil and tension of geogrids were recorded at the end of construction, and 5 years, 10 years and 15 years afterwards.

6.1. Results of numerical model

Fig. 14 shows the lateral displacement of retaining wall along wall height. The deformation in the middle of the wall was relative large, and the shape of the wall was similar to parabola. At the end of construction, the largest lateral displacement was 1.29 cm, which was taken place at 0.15 times the wall height (0.15H). After 5 years, 10 years, and 15 years, the largest lateral displacements were 2.93 cm, 3.49 cm and 3.88 cm, which were taken place at 0.5H, 0.53H and 0.58H, relatively. The lateral displacement almost unchanged at the base and gradually increased with time at top of the wall.

The surface settlement of the backfill soil at different moments is shown in Fig. 15. At the end of construction, settlement of reinforced area was less than the unreinforced area due to obvious effect of reinforcement. However, the increasing settlement of reinforced area was observed after construction. This is because plastic yielding behavior of soil was appeared within fracture surface of retaining wall, and the interaction of geogrids creep and soil creep amplified the overall creep effect of retaining wall. After 15 years, the settlement was about 3 cm compared to the end of construction. It indicates that the performance of reinforced retaining wall is able to adapt to the deformation of deep soft soil foundation.

Fig. 16 shows the surface settlement of the foundation soil. At the end of construction, the surface of foundation soil hunched

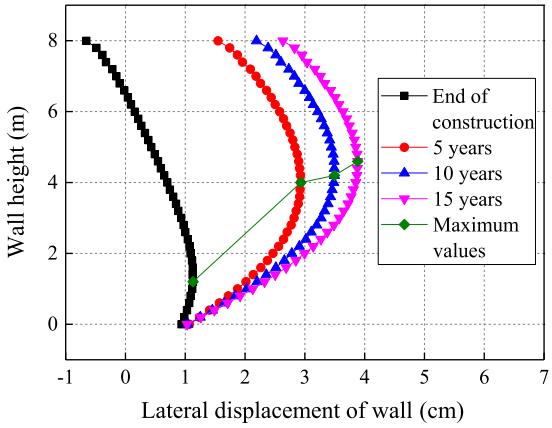

Fig. 14. Lateral displacement of wall at different moments.

Table 4
Model parameters of backfill and foundation soils.

Soil layer	Thickness/m	E/MPa	ν	ρ/kg·m^{-3}	β/(°)	Ψ/(°)	d/kPa	σ_c^0 /kPa	Parameters of creep model		
									A	m	n
Backfill soil	–	40	0.3	2000	40.893	0	24	33.74	1.28E−05	−0.735	0.856
Hard crust	0.8	20	0.3	1900	–	–	–	–	–	–	–
Soft soil	10	8	0.3	1650	36.204	0	12.558	16.611	9.32E−04	−0.72	1.635
Stiff clay	1.3	35	0.3	1800	–	–	–	–	–	–	–
Sand	1.75	42	0.3	1950	–	–	–	–	–	–	–
Weathering remaining soil	10	32	0.3	1850	–	–	–	–	–	–	–

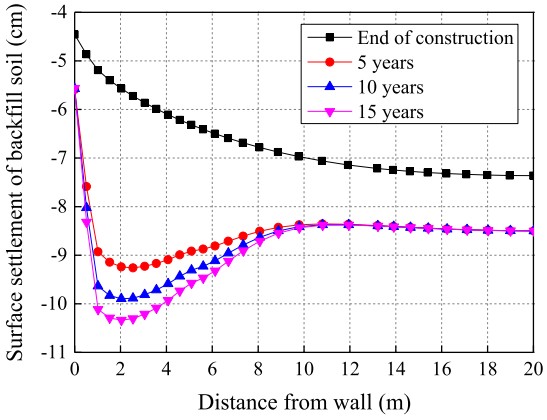

Fig. 15. Surface settlement of backfill soil at different moments.

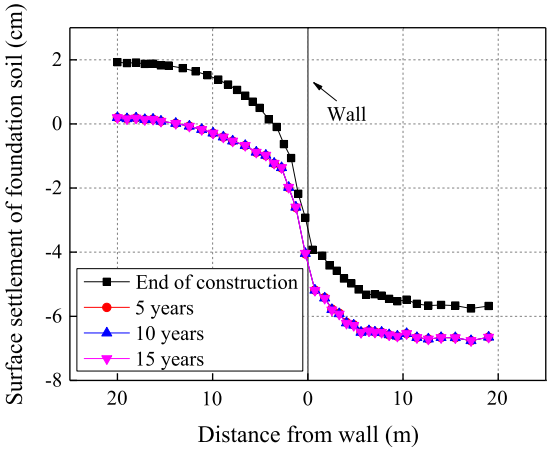

Fig. 16. Surface settlement of foundation soil at different moments.

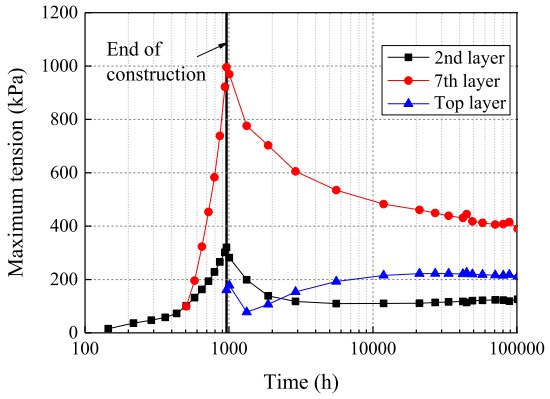

Fig. 17. Maximum tensions of geogrids at different layers.

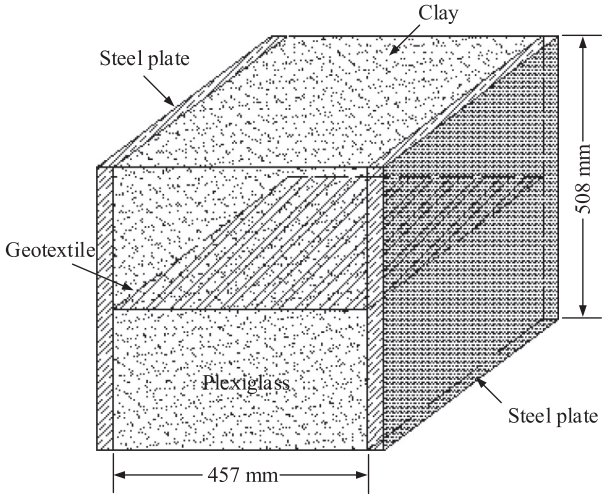

Fig. 18. Schematic diagram of test (Wu et al. (1996) [30]).

up at the left side of retaining wall and subsidence at the right side. After 5 years, the surface settlement was almost invariant. It indicates that consolidation deformation of soft soil foundation is the main factor affecting the deformation of retaining wall, and creep deformation of soft soil was not occurred due to most of upper loads were undertaken by piles. Therefore, the deep soft soil foundation which is treated by piles can ignore the creep behavior of soft soil.

The maximum tensions of geogrids at 2nd layer, 7th layer and top layer are shown in Fig. 17. For the 2nd layer and 7th layer, the maximum tensions increased with time during construction and decreased gradually over time and finally become stable after construction. This is likely because the active earth pressure induced by surcharge loading result in increasing tension in geogrids during construction and part of the tension transferred to adjacent soil, leading to decrease of tension in geogrids with time after construction. For the geogrids at top layer, the maximum tension decreased first. However, the maximum tension of geogrid increased gradually and then became stability due to the soil creep was greater than the geogrid creep deformation. Additionally, the maximum tension was appeared at 7th layer, and this trend also can be seen in Fig. 14. It indicates that high strength geogrids should be adopted at mid portion of retaining wall or spacing of geogrid reinforced layer should be reduced.

6.2. Validation of numerical model

A long-term creep behavior test of soil-geosynthetic composites, which was reported by Wu et al. [30], was used to validate the efficiency of numerical model. In this test, a 508-mm-high and 457-mm-wide reinforced soil unit consisted of 0.02-mm-thick geotextile reinforcement, two 1-mm-thick vertical flexible steel plates, and confining clay was placed inside a rigid container with transparent plexiglass side walls. The schematic diagram of test is shown in Fig. 18 and relative parameters can be found in Wu et al. [30,31]. The placement of soil layers was divided in two steps. In step 1, the surcharge of 45 kN/m^2 was used to consolidate the first layer clay for 26 days and then placed a sheet of the geotextile on top of the first layer soil. In step 2, the second layer of clay was placed on top of the geotextile, and the consolidation pressure of 45 kN/m^2 was applied at the top of second layer of clay for another 32 days [30]. After step 2, long-term performance of soil-geosynthetic composites began to monitor for 23,000 min.

In the numerical model, the steel plates were assumed to be linear elastic and the interface of plates and clay was using interface friction model. The geotextile was simulated using aforementioned constitutive model and clay was modeled using modified Drucker-Prager creep model, and the parameters of creep model were listed in Table 5. Only one-half of the geometry was analyzed due to symmetry [31].

Figs. 19 and 20 show the comparison between tested and calculated displacement at mid-point of steel plate and geotextile strain at different moments. It can be seen that the data obtained from test and model calculation were similar. There was a

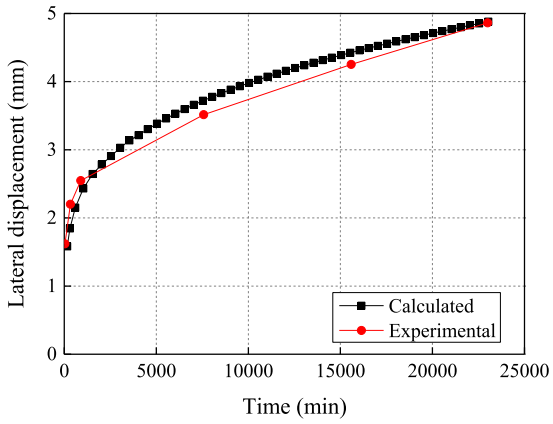

Fig. 19. Tested and calculated lateral displacement at mid-point of steel plate.

Table 5
Parameters of creep model.

Layer	A	m	n
Clay	2.521e−5	−0.827	1.094
Geotextile	2.748e−6	−0.872	0.686

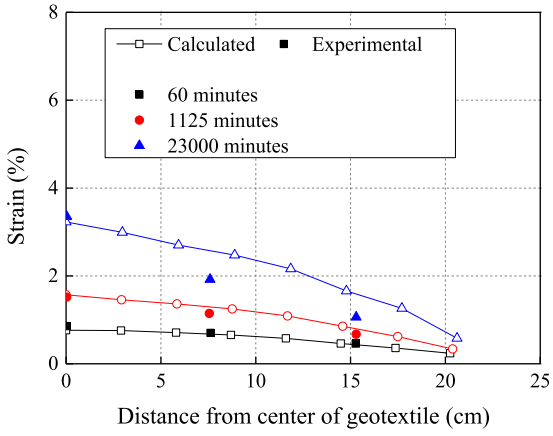

Fig. 20. Tested and calculated geotextile strain at different moments.

difference between the tested and predicted strain, however, the maximum difference value of strain was only 0.66%. Therefore, the numerical model has the capacity to simulate the creep behavior and deformation of geosynthetic reinforced retaining wall.

7. Conclusion

In this paper, creep behavior and stress relaxation of geogrids were discussed and a constitutive model was established based on creep tests. On this basis, long-term characteristics of a grogrids reinforced soil retaining wall were studied using finite element analysis. The following remarks can be made:

(1) Geogrids have the largest creep rate under different load levels at the beginning of load application, and the creep rate decreases and becomes stable gradually after certain period of time. The creep strains increase with the increasing load levels and the stress relaxation curves have the similar trend at different strains. To ensure the stability of the retaining wall, the working stress of geogrids should be less than 40% of ultimate tensile strength.

(2) The constitutive model for creep behavior and stress relaxation of geogrid is validated using the experimental data. The model is in good qualitative agreement with experimental data under different load levels.

(3) After construction, maximum tension of geogrids at the top layer increases with time, and other layers show obvious stress relaxation. The lateral displacement of the reinforced soil retaining wall increases gradually with time and presents a characteristic of larger in the middle of the wall and smaller at two ends, and the position of maximum lateral displacement obviously go up along the wall with time. This indicates that high strength geogrids should be adopted in the middle of retaining wall or the spacing of geogrid reinforced layers should be reduced.

(4) Consolidation deformation of soft soil foundation is the main factor affecting the deformation of retaining wall and the influence of secondary consolidation deformation is relative small. The deep soft soil foundation which is treated by piles can ignore the creep behavior of soft soil.

Acknowledgements

The authors wish to acknowledge the financial support to this study from the National Nature Science Foundation of China (No. 50808086) and thank the fund by China Scholarship Council as well as the support by innovation fund of South China University of Technology for excellent Ph.D. dissertations.

References

[1] S.S. Yeo, Y.G. Hsuan, Evaluation of creep behavior of high density polyethylene and polyethylene-terephthalate geogrids, Geotext. Geomembr. 28 (5) (2010) 409–421, http://dx.doi.org/10.1016/j.geotexmem.2009.12.003.
[2] R.J. Bathurst, Y. Miyata, Reliability-based analysis of combined installation damage and creep for the tensile rupture limit state of geogrid reinforcement in Japan, Soils Found. 55 (2) (2015) 437–446, http://dx.doi.org/10.1016/j.sandf.2015.02.017.
[3] H. Liu, H.I. Ling, Unified elastoplastic-viscoplastic bounding surface model of geosynthetics and its applications to geosynthetic reinforced soil-retaining wall analysis, J. Eng. Mech. 133 (7) (2007) 801–815, http://dx.doi.org/10.1061/(ASCE)0733-9399(2007) 133:7(801).
[4] G.Q. Yang, H. Liu, Y.T. Zhou, et al., Post-construction performance of a two-tiered geogrid reinforced soil wall backfilled with soil-rock mixture, Geotext. Geomembr. 42 (2) (2014) 91–97, http://dx.doi.org/10.1016/j.geotexmem.2014.01.007.
[5] G. Yang, B. Zhang, P. Lv, et al., Behaviour of geogrid reinforced soil retaining wall with concrete-rigid facing, Geotext. Geomembr. 27 (5) (2009) 350–356, http://dx.doi.org/10.1016/j.geotexmem.2009.03.001.
[6] C.V.S. Benjamim, B.S. Bueno, J.G. Zornberg, Field monitoring evaluation of geotextile-reinforced soil-retaining walls, Geosynthetics Int. 14 (2) (2007) 100–118, http://dx.doi.org/10.1680/gein.2007.14.2.100.
[7] M.M. Al-Hussaini, E.B. Perry, Field experiment of reinforced earth wall, J. Geotech. Eng. Div. 104 (3) (1978) 307–322.
[8] M.D. Bolton, P.L.R. Pang, Collapse limit states of reinforced earth retaining walls, Geotechnique 32 (4) (1982) 349–367, http://dx.doi.org/10.1680/geot.1982.32.4.349.
[9] B.R. Christopher, C. Bonczkiewicz, R. Holtz, Design, construction and monitoring of full scale test of reinforced soil walls and slopes, Recent Case Histories of Permanent Geosynthetic-Reinforced Soil Retaining Walls, 11, 1994, pp. 45–59.
[10] V. Elias, P.E. Barry, R. Christopher, Mechanically Stabilized Earth Walls and Reinforced Soil Slopes Design and Construction Guidelines, US Department of Transportation, Federal Highway Administration, 1997.
[11] M. Simac, R.J. Bathurst, R.R. Berg, et al., Design Manual for Segmental Retaining Walls, third ed., Herndon, Virginia, USA, 2010.
[12] J.F. Xue, J.F. Chen, J.X. Liu, et al., Instability of a geogrid reinforced soil wall on thick soft Shanghai clay with prefabricated vertical drains: a case study, Geotext. Geomembr. 42 (4) (2014) 302–311, http://dx.doi.org/10.1016/j.geotexmem.2014.05.003.
[13] M. Riccio, M. Ehrlich, D. Dias, Field monitoring and analyses of the response of a block-faced geogrid wall using fine-grained tropical soils, Geotext. Geomembr. 42 (2) (2014) 127–138, http://dx.doi.org/10.1016/j.geotexmem.2014.01.006.

[14] T. Nakajima, N. Toriumi, H. Shintani, et al., Field performance of a geotextile reinforced soil wall with concrete facing blocks, Earth Reinforcement (1996) 427–432.
[15] G.D. Skinner, R.K. Rowe, Design and behaviour of a geosynthetic reinforced retaining wall and bridge abutment on a yielding foundation, Geotext. Geomembr. 23 (3) (2005) 234–260, http://dx.doi.org/10.1016/j.geotexmem.2004.10.001.
[16] G. Raumann, A plane strain hydraulic tensile test for geotextiles, Matériaux et Construction 14 (4) (1981) 295–302, http://dx.doi.org/10.1007/BF02473949.
[17] C.C.H.C.M. Kwok, Parametric studies of the behaviour of a reinforced embankment, Geotext. Geomembr. Relat. Prod. 1 (1990) 137, http://dx.doi.org/10.1016/0148-9062(91)91531-U.
[18] J.A. Finnigan, The creep behavior of high tenacity yarns and fabrics used in civil engineering applications, in: Proceedings of the International Conference on the Use of Fabrics in Geotechnics, Paris, 2, 1977, pp. 305–309.
[19] R.F. Wilson-Fahmy, R.M. Koerner, Finite element modelling of soil-geogrid interaction with application to the behavior of geogrids in a pullout loading condition, Geotext. Geomembr. 12 (5) (1993) 479–501, http://dx.doi.org/10.1016/0266-1144(93)90023-H.
[20] C.T. Gnanendran, A.P.S. Selvadurai, Strain measurement and interpretation of stabilising force in geogrid reinforcement, Geotext. Geomembr. 19 (3) (2001) 177–194, http://dx.doi.org/10.1016/S0266-1144(01)00004-8.
[21] W.N. Findley, 26-Year creep and recovery of poly (vinyl chloride) and polyethylene, Polym. Eng. Sci. 27 (8) (1987) 582–585, http://dx.doi.org/10.1002/pen.760270809.
[22] B.M. Das, Creep behavior of geotextiles, Geotext. Geomembr. Relat. Prod. 2 (1990) 677–678.
[23] A. Sawicki, A basis for modelling creep and stress relaxation behaviour of geogrids, Geosynthetics Int. 5 (6) (1998) 637–645, http://dx.doi.org/10.1680/gein.5.0139.
[24] A. Sawicki, K. Kazimierowicz-Frankowska, Creep behaviour of geosynthetics, Geotext. Geomembr. 16 (6) (1998) 365–382, http://dx.doi.org/10.1016/s0266-1144(98)00020-x.
[25] ASTM D6637/D6637M-15, Standard Test Method for Determining Tensile Properties of Geogrids by the Single or Multi-Rib Tensile Method, ASTM International, West Conshohocken, PA, 2015.
[26] H. Hibbitt, B. Karlsson, P. Sorensen, Abaqus Analysis User's Manual Version 6.10, Dassault Systèmes Simulia Corp., Providence, RI, USA, 2011.
[27] Z. Cai, R.J. Bathurst, Seismic response analysis of geosynthetic reinforced soil segmental retaining walls by finite element method, Comput. Geotech. 17 (4) (1995) 523–546, http://dx.doi.org/10.1016/0266-352X(95)94918-G.
[28] R.K. Rowe, G.D. Skinner, Numerical analysis of geosynthetic reinforced retaining wall constructed on a layered soil foundation, Geotext. Geomembr. 19 (7) (2001) 387–412, http://dx.doi.org/10.1016/S0266-1144(01)00014-0.
[29] A. Singh, J.K. Mitchell, General stress-strain-time function for soils, J. Soil Mech. Found. Div. ASCE 94 (1) (1968) 21–46.
[30] J.T.H. Wu, S.M.B. Helwany, A performance test for assessment of long-term creep behavior of soil-geosynthetic composites, Geosynthetics Int. 3 (1) (1996) 107–124, http://dx.doi.org/10.1680/gein.3.0056.
[31] S.M.B. Helwany, J.T.H. Wu, A numerical model for analyzing long-term performance of geosynthetic-reinforced soil structures, Geosynthetics Int. 2 (2) (1995) 429–453.
[32] Liu. Huabei, Wang. Xiangyu, Song. Erxiang, Long-tern behavior of GRS retaining walls with marginal backfill soils, Geotext. Geomembr. 27 (2009) 295–307.